

Comprehensive Analysis of Maximum Power Association Policy for Cellular Networks Using Distance and Angular Coordinates

Charalampos (Harris) K. Armeniakos, *Graduate Student Member, IEEE*,

Athanasios G. Kanatas, *Senior Member, IEEE*,

and Harpreet S. Dhillon, *Fellow, IEEE*

Abstract

A novel stochastic geometry framework is proposed in this paper to study the downlink coverage performance in a millimeter wave (mmWave) cellular network by jointly considering the polar coordinates of the Base Stations (BSs) with respect to the typical user located at the origin. Specifically, both the Euclidean and the angular distances of the BSs in a maximum power-based association policy for the UE are considered to account for realistic beam management considerations, which have been largely ignored in the literature, especially in the cell association phase. For completeness, two other association schemes are considered and exact-form expressions for the coverage probability are derived. Subsequently, the key role of angular distances is highlighted by defining the dominant interferer using angular distance-based criteria instead of Euclidean distance-based, and conducting a dominant interferer-based coverage probability analysis. Among others, the numerical results revealed that considering angular distance-based criteria for determining both the serving and the dominant interfering BS, can approximate the coverage performance more accurately as compared to utilizing Euclidean distance-based criteria. To the best of the authors' knowledge, this is the first work that rigorously explores the role of angular distances in the association policy and analysis of cellular networks.

Index Terms

C. K. Armeniakos and A. G. Kanatas are with the Department of Digital Systems, University of Piraeus, 18534 Piraeus, Greece (e-mail: {harmen,kanatas}@unipi.gr).

H. S. Dhillon is with with Wireless@Virginia Tech, Bradley Department of Electrical and Computer Engineering, Virginia Tech, Blacksburg, 24061, VA, USA (e-mail: hdhillon@vt.edu).

6G, 5G NR, beam management, coverage probability, millimeter-wave communication, Poisson point process, stochastic geometry.

I. INTRODUCTION

Due to the rapid proliferation of the smart devices and novel rate-greedy applications, mobile data traffic has witnessed a tremendous growth. As the fifth generation (5G) cellular networks become more ubiquitous and we start thinking of the sixth generation (6G), the networks will continue to expand to higher frequency bands to address the need for extreme capacity. Recently, millimeter wave (mmWave) and sub-Terahertz (THz) networks, operating at frequencies between 24 and roughly 330 GHz, have attracted considerable attention from both academia and industry due to the enormous available bandwidth [1], [2]. However, the extremely high data rates achieved in mmWave and sub-THz bands come with challenging propagation characteristics, with the path loss being a key issue. To overcome these limitations, first, mmWave networks are envisioned to be densely deployed to achieve acceptable coverage [3]. However, increasing the density of base stations (BSs) leads to severe interference problems. Next, steerable antenna arrays with highly directional antenna beams are needed to achieve high power gain and improved coverage. The resulting interference may cause a significant number of transmission failures, especially for dense mmWave networks [3]. Therefore, the antennas' 3 dB beamwidth becomes a key design parameter. In addition, mmWave channels are sensitive to the dynamically changing propagation environment (moving pedestrians, passing cars, blockages, etc.). Thus, 5G New Radio (NR) mmWave wireless networks rely on adaptive beamforming and beam selection techniques for optimizing the performance.

In a network where the user equipment (UEs) and the BSs are equipped with antenna arrays that are able to form directional beams, one of the most rational criteria utilized to perform the association of the UE to a serving BS is that of the maximum received power. Therefore, the probability density function (pdf) of the desired signal received power should be calculated based on both polar coordinates. As we will discuss shortly, if one ignores practical beam management considerations, cell association decisions can be made purely based on the Euclidean distances. However, in this paper, it is rigorously argued that if one accounts for these realistic considerations, one additionally needs to consider angular distances. Inspired by this, we present the first comprehensive analysis of maximum power association policy that takes into account both the Euclidean and angular distances.

A. Related Work and Motivation

With the rise of 5G and beyond communication systems, the use of multiple antennas at the BSs and the UEs has introduced beamforming capabilities as a central feature in 5G NR that leads to higher data rates. However, a series of beam management procedures are needed to ensure efficient handling and network operation. The selection of the best receiving beam is performed by measuring the average received signal power in each beam through exhaustive scanning in a set of candidate serving BSs. The maximum power-based association policy is governed by the distance dependent path loss and the transmitting and receiving antenna gain patterns. However, either a binary valued antenna pattern, called flat-top pattern [4]–[6], or ideal conditions with realistic patterns, i.e., perfect channel estimation and beam training, that imply full alignment between BS’s transmitting and UE’s receiving beams has been assumed in most cases. In this *ideal baseline scenario*, the cell association decision is purely based on the Euclidean distance of the two nodes [3], [7]–[12].

In this direction, many works in the literature have studied beam management techniques and procedures for 5G NR networks by adopting tools from stochastic geometry, since it captures the spatial randomness of network elements [13]–[15]. Modeling the spatial locations of BSs and/or UEs as point processes allows the use of powerful tools from stochastic geometry to derive tractable analytical results for several key performance metrics. Therefore, in [16], the authors study among others both the initial beam selection during BS handover and beam reselection technique in a mmWave cell. However, the interference from other BSs is ignored. To address this issue, the authors in [17] develop a stochastic geometry framework and conduct a detailed performance analysis in terms of the average achievable rate and success probability. Going beyond the coverage probability and the achievable rate, in [18], the authors studied the average number of beam switching and handover events, in mmWave vehicular networks. Several beam management techniques were also considered. In [19], the authors investigated the impact of beamwidth, mobility, blockage, and molecular absorption in the reliability and throughput of a THz network. The impact of the highly directional antennas on the beam management procedures, was also addressed.

In realistic mmWave networks, beam misalignment is inevitable, and the direction of the UE’s maximum gain may not be necessarily fully aligned with the corresponding one of the serving BS [20]. In this case, the misalignment error, which is now a function of the angular distance

between the candidate serving BSs and the UE, should be considered in the measurement of the received power during the UE's association policy. The authors in [21] and [10] model the misalignment error as a random variable following the truncated Gaussian distribution, whereas the authors in [22], derived an empirical pdf for the misaligned gain based on simulations. To the best of the authors' knowledge, this work proposes for the first time a stochastic geometry framework to study the performance in a mmWave cellular network by adopting 5G NR beam management-based procedures and jointly considering the impact of both the Euclidean and angular distances of the BSs in the UE's association policy. The use of the angular distance is critical for the accurate estimation of the receiving antenna gain using realistic 3GPP antenna patterns and allows to depart from the ideal baseline scenario.

Along similar lines, many works have captured the effect of the angular coordinate in the calculation of interference power and correspondingly in performance analysis of cellular networks by adopting realistic antenna patterns. In [23], the authors considered the effect of beam misalignment utilizing a 3GPP-based antenna pattern in a stochastic geometry framework. In [24], the authors investigate the impact of directional antenna arrays on mmWave networks. Among other insights, the role of realistic antenna patterns in the interference power is demonstrated. In [25], a multi-cosine antenna pattern is proposed to approximate the actual antenna pattern of a uniform linear array (ULA) and the impact in the interference power is highlighted. In [26], the authors adopt an actual three dimensional antenna model and a uniform planar array, which is mounted on UAVs, to examine the impact of both azimuth and elevation angles on the interference power.

On another front, the idea of the dominant interferer has been introduced in the literature to facilitate the calculation of the SINR and provide a realistic and mathematically tractable approximation of the accurate aggregate interference [27]–[30]. The notion of angular distances and their implication on the identification of the dominant interferer has recently been highlighted in [31] and [32]. Accordingly, a dominant interfering BS may not necessarily be the closest one to the receiver. Indeed, a far interferer may cause more severe interference than a closer one, due to the fact that the Angle-of-Arrival (AoA) at the receiver may fall within the 3dB beamwidth of the antenna beam.

In summary, even though angular coordinates have appeared in the stochastic geometry-based analysis, their manifestation in the received power as a consequence of realistic beam management procedure and the overall effect on the system performance has not been studied,

which is the main objective of this paper. Consequently, this work proposes for the first time a stochastic geometry framework to study the implications of beam misalignment error in the association policy and the corresponding performance of a mmWave cellular network by adopting realistic 5G NR beam management-based procedures. Therefore, extended comparison of the ideal baseline scenario with several association policies is provided, and evaluation of diverse dominant interferer-based scenarios are highlighted.

B. Contributions

The main contributions of this paper are the following:

1) *Angular distance distributions*: By exploiting fundamental concepts of stochastic geometry theory, both the n th nearest node and joint angular distance distributions within a finite ball are derived in closed form for a two-dimensional (2D) finite homogeneous Poisson point process (HPPP). As it will be shown, these distances play a key role in the definition of dominant interferer in mmWave networks.

2) *Refining the maximum power association policy in a mmWave stochastic geometry framework*: By employing the HPPP for modeling the spatial locations of the BSs, a number of BSs with known density is deployed in a mmWave cellular network. The typical UE, which is equipped with a realistic 3GPP-based antenna pattern, exploits directional beamforming capabilities under imperfect alignment to communicate with the serving BS. To this end, as a key contribution, a realistic beam management-based association policy that jointly considers both the Euclidean and angular distances of the BSs, is proposed for the UE. The proposed novel policy takes into account both the directional beamforming and the beam misalignment error at the UE through the adoption of a 3GPP-based antenna pattern. Two other association schemes, i.e., an ideal baseline scenario and a purely angular distance-based association scheme, are also proposed as special cases for completeness.

3) *Coverage probability analysis*: Performance analysis in terms of coverage probability is conducted under the three association schemes and analytical expressions are obtained. As key intermediate results, the pdf of the maximum received power and the Laplace transform (LT) of the aggregate interference power distributions, are derived in exact form.

4) *Dominant interferer approach*: Conventionally, the dominant interferer is considered as the nearest BS in Euclidean distance. By extending the definition of the dominant interferer as the nearest BS in angular distance w.r.t. a reference line in mmWave networks, coverage probability

analysis is conducted for the two special cases under the assumption of a dominant interferer and exact-form expressions are derived. To this end, the pdf of the ratio of the nearest BS, in angular distance, antenna gain to that of the second nearest BS, as well as the pdf of the ratio of the corresponding path-losses are derived as insightful intermediate results. Subsequently, the corresponding analytical expressions for the cumulative distribution function (cdf) of the achieved signal-to-interference ratio (SIR) are obtained in exact form.

The remainder of the paper is organized as follows. In Section II, the angular distance distributions in a 2D finite HPPP are derived as preliminaries. In Section III, the system model is analytically presented and both the association policies and the beam selection schemes for the UE are proposed. In Section IV, the coverage probability analysis under the three association schemes, is presented while in Section V, the coverage probability analysis is conducted under the dominant interferer assumption. Section VI presents both the analytical and the numerical results, while Section VII concludes the paper.

II. MATHEMATICAL PRELIMINARY: ANGULAR DISTANCES

In this section, the mathematical constructs of angular distances in 2D HPPP wireless networks, are presented. These will provide a firm foundation in the understanding and analysis of the coverage probability in mmWave cellular networks.

A. Angular Distance Distributions

As stated in [31], the investigation of the distributions of the angular distances is based on defining the n th nearest point in angle ϕ from a reference line. Consider a homogeneous PPP $\Phi \subset \mathbb{R}^2$ with intensity λ . Let ϕ_n denote the random variable representing the angular distance from an arbitrary reference line to the n th nearest point of Φ in the coordinate ϕ , as shown in Fig. 1a. Without loss of generality, the reference line is assumed to be the x -axis. Then, the pdf of the n th nearest point in angular distance conditioned on its Euclidean distance being smaller than r , is given by

$$f_{\phi_n|r}(\phi|r) = \frac{(\lambda\phi r^2)^n}{2^n\Gamma(n)\phi} e^{-\frac{\lambda\phi r^2}{2}}, \quad r > 0, \phi \in [0, 2\pi], \quad (1)$$

where $\Gamma(\cdot)$ is the Gamma function defined as in [33, eq. (8.310.1)]. This conditioning on the distance will be useful when we apply this result to the mmWave setting shortly.



Fig. 1: The n th nearest point in angular distance in a disk sector.

Proof. Let $W(\phi, r)$ denote a disk sector with dihedral angle ϕ and radius r . The area of the disk sector is $|W(\phi, r)| = \frac{\phi r^2}{2}$. Following the Poisson distribution, the probability that k points fall in $W(\phi, r)$ is given by

$$\mathbb{P}[k \text{ points in } W(\phi, r)] = \frac{(\lambda |W(\phi, r)|)^k}{k!} e^{-\lambda |W(\phi, r)|}. \quad (2)$$

Then, the complementary cdf (ccdf) of ϕ_n is given by

$$\begin{aligned} S_n &= \mathbb{P}[\phi_n > \phi | r] \\ &= \mathbb{P}[\text{Number of points in } W(\phi, r) < n] \\ &= \sum_{k=0}^{n-1} \mathbb{P}[k \text{ points in } W(\phi, r)] = \frac{\Gamma(n, \lambda |W(\phi, r)|)}{\Gamma(n)}, \end{aligned} \quad (3)$$

where $\Gamma(\cdot, \cdot)$ denotes the incomplete gamma function defined as in [33, eq. (8.350.2)]. Now, $f_{\phi_n|r}(\phi|r)$ can be obtained by taking the derivative of an incomplete gamma function w.r.t to the angle ϕ , given by $f_{\phi_n|r}(\phi|r) = -\frac{\partial S_n}{\partial \phi}$, which results in (1). ■

In mmWave cellular networks, it is often of interest the absolute angular distance, $|\phi|$, for the coordinate ϕ . This definition is particularly useful when dealing with angular distances from the direction of the maximum directivity in an antenna beam pattern [31]. Let $|\phi| \in [0, \pi]$, as shown in Fig. 1b. Accordingly, the pdf $f_{|\phi_n||r}(|\phi||r)$ is given by

$$f_{|\phi_n||r}(|\phi||r) = \frac{(\lambda |\phi| r^2)^n}{\Gamma(n) |\phi|} e^{-\lambda |\phi| r^2}, \quad r > 0, |\phi| \in [0, \pi]. \quad (4)$$

Proof. Letting $\phi = 2|\phi| \in [0, 2\pi]$, then $W(|\phi|, r) = |\phi| r^2$. Then, the proof follows the same steps as the proof for obtaining (1). ■

B. Joint Distributions

As mentioned in Section I.A, a UE may now be connected to the closest BS in angular distance. In this case, the dominant interfering BS may not necessarily be the closest one to the UE, but the closest BS in angular distance w.r.t the line of communication link. This inspires the investigation of joint distributions of angular distances.

Let $|\varphi_n|$ denote the absolute angular distance from o to the n th nearest point in absolute angular distance. Then, the joint pdf of $|\varphi_1|, |\varphi_2|$ is given by

$$f_{|\varphi_1|, |\varphi_2||r}(|\varphi_1|, |\varphi_2||r) = (\lambda r^2)^2 e^{-\lambda r^2 |\varphi_2|}, \quad (5)$$

where $|\varphi_1| \in [0, \pi]$, $|\varphi_2| \in [|\varphi_1|, \pi]$ and $r > 0$.

Proof. See Appendix A. ■

III. SYSTEM MODEL

This section presents the considered mmWave cellular network and the key modeling assumptions.

A. Network Model

Consider a mmWave downlink cellular network, where the locations of the BSs is modeled as a HPPP $\Phi_{bs} \subset \mathbb{R}^2$ with intensity λ_{bs} . Let (r_x, ϕ_x) denote the location of a BS located at $x \in \Phi_{bs}$, in terms of polar coordinates. The locations of UEs are independently distributed according to some stationary point process Φ_{ue} . Also, a BS serves one UE at a time per resource block and all BSs are assumed to transmit at the same power p . Let (r_s, ϕ_s) denote the location of the serving BS $x_0 \in \Phi_{bs}$ at a given time. Without loss of generality, the receiving UE is assumed to be located at the origin $\mathbf{o} = (0, 0)$ at that time. After averaging the performance of this UE over Φ_{bs} , the receiving UE becomes the typical receiver, or simply *receiver*.

B. Beamforming and Antenna Modeling

A BS located at $x \in \Phi_{bs}$ is assumed to exploit beamforming techniques to communicate with the receiver. Therefore, the maximum gain of the BSs' antennas is assumed to be always directed towards the receiver, for the sake of mathematical tractability. The receiver is assumed to be equipped with an antenna array able to produce 2^m receiving beams. The maximum gain directions of these beams, i.e., the centers of the corresponding 3 dB beamwidths, are given

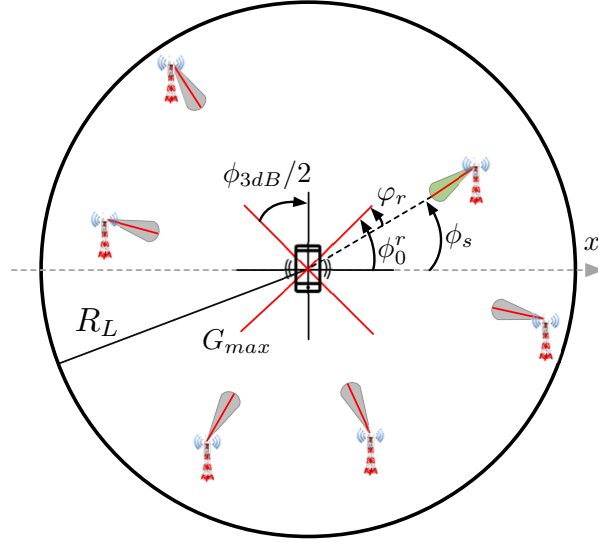


Fig. 2: Illustration of the system model.

by $\phi_m = \frac{2\pi}{2^m}$ with $m \in \mathbb{N}$. Please note that the maximums of the BS and UE beams will not necessarily be aligned because of the discretization on the UE side, which is the reason angular distances appear in the analysis. In this work, a realistic 3GPP-based antenna pattern recommended for 5G mmWave communications [34] is adopted for the receiver and therefore, the actual antenna gain within the 3dB beamwidth range is not constant. When directed towards ϕ_0^r , this antenna has a radiation power pattern (in dB) given by

$$G_{3gpp}(\phi - \phi_0^r) = G_{max} - \min \left\{ 12 \left(\frac{\phi - \phi_0^r}{\phi_{3dB}} \right)^2, SLA \right\}, \quad (6)$$

where ϕ_{3dB} is the 3dB beamwidth of the receiver's antenna and $SLA = 30\text{dB}$ is the front-to-back ratio. The multiplicative antenna gain factor is denoted by $g_{3gpp}(\phi - \phi_0^r)$. In this work, the direction of maximum gain ϕ_0^r is modeled as a discrete random variable with probability mass function (pmf) given by

$$\phi_0^r = \begin{cases} \phi_0^1 = \frac{\pi}{2^m}, & \text{w.p. } p_\phi = \frac{1}{2^m} \\ \phi_0^2 = \frac{\pi}{2^m} + \frac{\pi}{2^{m-1}}, & \text{w.p. } p_\phi = \frac{1}{2^m} \\ \vdots & \\ \phi_0^{2^m} = \frac{\pi}{2^m} + \underbrace{\frac{\pi}{2^{m-1}} + \dots + \frac{\pi}{2^{m-1}}}_{(2^m-1) \text{ terms}}, & \text{w.p. } p_\phi = \frac{1}{2^m} \end{cases}, \quad (7)$$

A representative example of ϕ_0^r is shown in Fig. 2, with $2^m = 4$ beams enabled at the UE. Unfortunately, performance analysis using the array pattern of (6) may lead to extremely intractable

analysis [24]. For this reason, the array pattern is approximated by the two-branch expression given by [35],

$$g(\phi - \phi_0^r) = \begin{cases} g_{max} 10^{-\frac{3}{10} \left(\frac{2(\phi - \phi_0^r)}{\phi_{3dB}} \right)^2}, & |\phi - \phi_0^r| \leq \phi_A \\ g_s, & \phi_A \leq |\phi - \phi_0^r| \leq \pi \end{cases}, \quad (8)$$

where g_{max} and g_s are the multiplicative gain factors of G_{max} , and $G_s = G_{max} - SLA$, correspondingly, whereas $\phi_A = (\phi_{3dB}/2) \sqrt{(10/3) \log_{10}(g_{max}/g_s)}$.

C. Blockage Model

As seen from the receiver location, a BS can be either LOS or non-LOS (NLOS). While mmWave signals are significantly affected by blockages [36], proper modeling is essential to capture the effect of blockages on network performance. In this work, an LOS ball model is adopted since it provides a better fit with real-world blockage scenarios [37]. Given a BS located at $x \in \Phi_{bs}$, the propagation between the BS and the receiver is LOS if $\|x\| < R_L$, where R_L is the maximum distance for LOS propagation and $\|\cdot\|$ denotes the Euclidean norm. The received signal power from the BSs outside the LOS ball is considered negligible due to the severe path loss imposed by the blockages [3], [38], and the authors in [39], have shown that NLOS links have negligible effect on the system coverage performance in dense mmWave networks. Hence, the performance analysis for the receiver is restricted to $\mathbf{b}(\mathbf{o}, R_L)$ ¹, where $\mathbf{b}(\mathbf{o}, R_L)$ denotes a LOS ball of radius R_L centered at the origin \mathbf{o} . Therefore, the analysis is restricted to the finite HPPP $\Psi_{bs} = x \in \Phi_{bs} \cap \mathbf{b}(\mathbf{o}, R_L)$.

D. Path Loss and Channel Models

Let α_L denote the path loss exponent for the LOS propagation links. Similar to [17], typical values of α_L are $\alpha_L \in [1.8, 2.5]$. Then, following the standard power-law path-loss model for the path between the receiver and a BS located at $x \in \Psi_{bs}$, the random path loss function is denoted by $l(\|x\|) = K\|x\|^{-\alpha_L}$, where $K = \left(\frac{c}{4\pi f_c}\right)^2$ with c being the speed of light and f_c the carrier frequency.

The channels between a BS located at $x \in \Psi_{bs}$ and the receiver undergo Nakagami- m_u fading, which is a generalized model for representing a wide range of fading environments. The

¹It is assumed that the density of the BSs is large enough so that there is always at least one BS within $\mathbf{b}(\mathbf{o}, R_L)$.

parameter m_u is restricted to integer values for analytical tractability. The channel fading gain h_u is the fading power for the channel in LOS condition. The shape and scale parameters of h_u are m_u and $1/m_u$, respectively, i.e., $h_u \sim \text{Gamma}(m_u, \frac{1}{m_u})$. Here, $u \in \{s, x\}$, where s denotes the link between the receiver and the serving BS, and x stands for the link between the receiver and the interfering BSs at $x \in \Psi_{bs} \setminus \{x_0\}$. The pdf of h_u is given by

$$f_{h_u}(w) = \frac{m_u^{m_u} w^{m_u-1}}{\Gamma(m_u)} \exp(-m_u w). \quad (9)$$

Note that $\mathbb{E}[h_u] = 1$, where $\mathbb{E}[\cdot]$ denotes expectation. Also, the values of m_s are restricted to integers for analytical tractability.

E. User Association and Beam Selection Policy

The association policy used in real networks is often based on the maximum received power. The UE is agnostic to the conditions that provide the maximum power to the receiver. One of the main contributions of this paper is the adoption of an association policy, namely *Policy 1*, that optimally captures the real conditions. This is achieved by jointly considering both polar coordinates in the calculation of received power. With the introduction of the angular coordinate, the authors investigate the use of a similar to the minimum Euclidean distance-based criterion, i.e., the minimum angular distance-based one. This is called *Policy 2* in the following. Nevertheless, for system performance analysis purposes it is widely accepted that simplified policies may be considered. Therefore, a commonly utilized policy, namely *Policy 3*, is the one that assumes only the Euclidean distance criterion (as has been done extensively in the literature under simplistic modeling assumptions). However, this policy ignores the effect of angle-dependent antenna gains and inherently imposes a discrepancy from real received power in the calculations. Consequently, Policies 2 and 3 serve as baseline schemes for comparison to Policy 1 which is the best approximation to the maximum power association scheme.

1) *Policy 1: Maximum Power-based Association Scheme*: In this scheme, the receiver is associated with the BS providing the largest average received power by jointly considering both the Euclidean and the angular distance of the BSs. Specifically, during this association procedure, the best receiving beam is selected by the receiver for reception. According to the beam management procedure in 5G NR, this task is the so-called beam selection procedure. In particular, all BSs periodically transmit the beamformed reference signals, either channel state information reference signals (CSI-RS) or synchronization signal blocks (SSBs), that may

cover the entire set of available directions according to the receivers' needs. The mmWave-based measurements for initial access are based on the SSBs. The receiver in the proposed framework monitors the reference signals and forms a list of *candidate serving BSs*, being those BSs with the largest SNR, if above a predefined threshold, for each beam. Subsequently, the *serving BS*, defined as the BS providing the largest SNR among *all* candidate serving BSs, is chosen for transmission. The corresponding receiver's beam in which the serving BS was identified, is selected as the *receiving beam*.

A key assumption in this policy is that the BS has perfect CSI knowledge of the uplink and thus, a perfect alignment of the BS beam maximum gain direction with the line toward the receiver is achievable. However, the direction of the maximum gain of the receiver's antenna is not fully aligned with the direction of maximum gain of each BS transmitting beam. Let φ_i^x denote the angular distance between the direction of the line connecting the receiver and a BS $x \in \Psi_{bs}$ and the direction, ϕ_0^i , of maximum directivity of a receiver's beam i . Therefore, for a BS $x \in \Psi_{bs}$, ϕ_x denotes its polar coordinate, and φ_i^x is given by $\varphi_i^x = |\phi_0^i - \phi_x|$. By further considering the Euclidean distances of the BSs from the origin, r_x , the location of the serving BS and the receiving beam are chosen by the receiver as

$$(x_0, i) = \underset{\substack{x \in \Psi_{bs} \\ i=1:2^m}}{\operatorname{argmax}} \left\{ g(\varphi_i^x) r_x^{-\alpha_L} \right\}, \quad (10)$$

Having selected x_0 and i , the angle φ_i^x is denoted as φ_r in Fig. 2. In this case, φ_r can be modeled as a uniform random variable, i.e., $\varphi_r \sim U[0, \frac{\phi_{3dB}}{2}]$, where ϕ_{3dB} denotes the half-power beamwidth of the user receiving beam. Clearly, the serving BS may not necessarily be the nearest one to the receiver. Instead, it may lie close to the direction of the maximum directivity gain of a receiver's beam and thus providing maximum received power. Eq. (10) indicates that the receiver performs scanning for each beam to identify the serving BS by jointly considering both the angular distance of the BSs, from the direction of each beam's maxima, and the Euclidean distance of the BSs, respectively to maximize the received power. Note that the serving BS can lie anywhere in $\mathbf{b}(\mathbf{o}, R_L)$.

2) *Policy 2: Minimum Angular Distance Association Scheme*: In this scheme, the receiver is attached to the closest BS in angular distance. Specifically, for each beam, the receiver performs exhaustive scanning and calculates the minimum angle between the direction of the beam's maxima and the direction of the line connecting the receiver and each BS. Then, from a list of 2^m angles, the receiver attaches to the BS with the minimum angular distance φ_c and the

corresponding beam is selected as the receiving beam. Mathematically, the location x_0 of the serving BS and the beam i are selected by the receiver as

$$(x_0, i) = \underset{\substack{x \in \Psi_{bs} \\ i=1:2^m}}{\operatorname{argmin}} \left\{ |\phi_0^i - \phi_x| \right\}, \quad (11)$$

and φ_c is given by

$$\varphi_c = \min_{i=1:2^m} \left\{ \min_{x \in \Psi_{bs}} \{ |\phi_0^i - \phi_x| \} \right\}. \quad (12)$$

3) *Policy 3: Minimum Euclidean Distance Association Scheme:* In this scheme, the receiver is associated with the nearest BS in Euclidean distance within $\mathbf{b}(\mathbf{o}, R_L)$. In this case, by adopting conventional beam management-based beam steering techniques, the maximum gain of the receiver's antenna is assumed to be directed towards the serving BS and therefore perfect beam alignment is assumed. Without loss of generality, due to the isotropy and the stationarity property of the Ψ_{bs} , the reference line can be considered to be along the x -axis and passing through the origin. In this case, the location x_0 of the serving BS is chosen by the receiver as $x_0 = \underset{x \in \Psi_{bs}}{\operatorname{argmin}} \{ r_x \}$.

F. Signal-to-interference-plus-noise Ratio

The SINR under the three association schemes is now defined. Under Policy 1, the received SINR is given by

$$\text{SINR} = \frac{p h_s g_{max} g(\varphi_r) l(\|x_0\|)}{I + \sigma^2}, \quad (13)$$

where p is the transmitted power and I refers to the aggregate interference power and is given by $I = \sum_{x \in \Psi_{bs}^!} p h_x g_{max} g_{3gpp}(\varphi_I) l(\|x\|)$, $\Psi_{bs}^! = \{ \Psi_{bs} \setminus \{x_0\} \}$, φ_I is defined as $\varphi_I = |\phi_0^r - \phi_x|$ and σ^2 is the additive white Gaussian noise power. Please note that, ϕ_0^r also determines the direction of the reference line in this policy.

Under Policy 2, the received SINR is given by

$$\text{SINR} = \frac{p h_s g_{max} g(\varphi_c) l(\|x_0\|)}{I + \sigma^2}, \quad (14)$$

where I is given by $I = \sum_{x \in \Psi_{bs}^!} p h_x g_{max} g_{3gpp}(\varphi_I) l(\|x\|)$ and φ_I is defined as $\varphi_I = |\varphi_c - \phi_x|$. Please note that, φ_c also determines the direction of the communication link in this policy.

Under Policy 3, the received SINR is given by

$$\text{SINR} = \frac{p h_s g_{max} g_{max} l(\|x_0\|)}{I + \sigma^2}, \quad (15)$$

where I is given by $I = \sum_{x \in \Psi_{bs}^!} p h_x g_{max} g_{3gpp}(\phi_x) l(\|x\|)$.

IV. COVERAGE PROBABILITY ANALYSIS

In this section, performance analysis in terms of coverage probability, $\mathcal{P}_c(\gamma) \triangleq \mathbb{P}(\text{SINR} > \gamma)$, is conducted under the three association schemes.

A. Coverage Probability Under Maximum Power Association Scheme

To obtain $\mathcal{P}_c(\gamma)$ in this scheme, the pdf of the maximum received power must first be derived. Let S_x^i denote the received power from a BS located at $x \in \Psi_{bs}$ measured w.r.t to the i -th beam. Then, S_x^i is given by

$$S_x^i = g(|\phi_0^i - \phi_x|) \|x\|^{-\alpha_L} = g(|\phi_0^i - \phi_x|) r_x^{-\alpha_L}. \quad (16)$$

and the maximum received power S is obtained as

$$S = \max_{\substack{x \in \Psi_{bs} \\ i=1:2^m}} \{S_x^i\} \stackrel{(a)}{=} \max_{x \in \Psi_{bs}} \underbrace{\{g(\varphi_r) r_x^{-\alpha_L}\}}_{S_x} \stackrel{(b)}{=} g(\varphi_r) r_s^{-\alpha_L}, \quad (17)$$

where (a) follows from the independence between ϕ_x and r_x of the BSs and maximization over $\{g(|\phi_0^i - \phi_x|)\}_{i=1:2^m}$ and (b) follows from maximization over $\{r_x^{-\alpha_L}\}_{x \in \Psi_{bs}}$ with $r_s = \|x_0\|$. Due to exhaustive scanning of the receiver in the whole $\mathbf{b}(\mathbf{o}, R_L)$, the serving BS may lie anywhere in $\mathbf{b}(\mathbf{o}, R_L)$. Therefore, the distances r_x are independent and identically distributed (i.i.d.) in $\mathbf{b}(\mathbf{o}, R_L)$ with pdf $f_{r_x}(r)$ of each element given by $f_{r_x}(r) = \frac{2r}{R_L^2}$, $r \in [0, R_L]$. The pdf of S can now be derived as intermediate result in the coverage probability analysis.

Lemma 1. *The pdf of the maximum received power S is given by*

$$f_S(s_0) = \lambda_{bs} \pi R_L^2 f_{S_x}(s_0) e^{\lambda_{bs} \pi R_L^2 \left(\int_{w_{min}}^{s_0} f_{S_x}(w) dw - 1 \right)}, \quad s_0 \in [w_{min}, \infty), \quad (18)$$

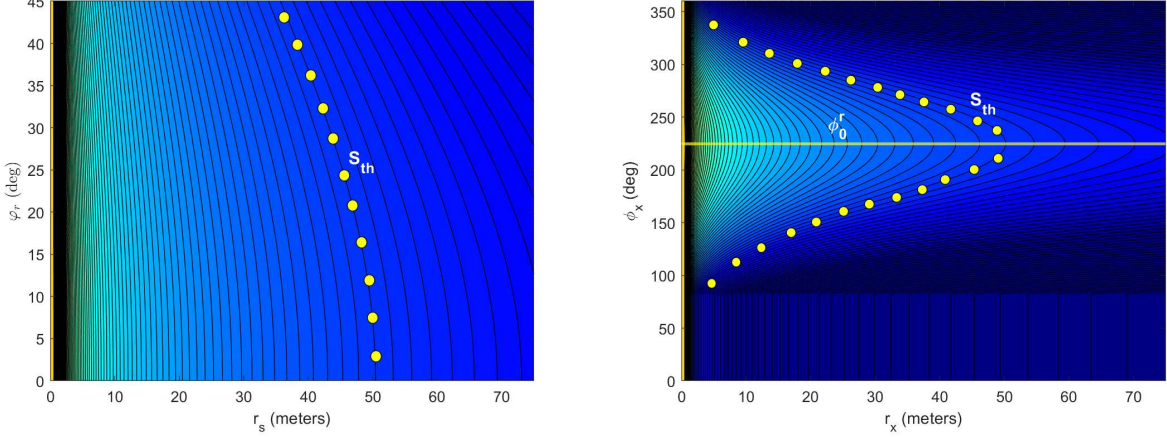
where $f_{S_x}(w)$ is given by

$$f_{S_x}(w) = \int_{g_{3dB}}^{\psi(w)} \frac{1}{x} f_{g(\varphi_r)}(x) f_{r_x^{-\alpha_L}}\left(\frac{w}{x}\right) dx, \quad w \in [w_{min}, \infty), \quad (19)$$

where $f_{r_x^{-\alpha_L}}(x) = \frac{2(\frac{1}{x})^{\frac{\alpha_L+2}{\alpha_L}}}{\alpha_L R_L^2}$, $f_{g(\varphi_r)}(g) = \frac{1}{\ln(10)x} \frac{10}{12 \sqrt{\frac{G_{max} - 10 \log(x)}{12}}}$, $g_{3dB} = 10^{\frac{G_{max} - 3}{10}}$, $w_{min} = g_{3dB} R_L^{-\alpha_L}$ and $\psi(w) = \min\left\{\frac{w}{R_L^{-\alpha_L}}, g_{max}\right\}$.

Proof. See Appendix B. ■

Having obtained the pdf of S , the conditional Laplace transform of the aggregate interference power distribution is now derived as a key intermediate result in the coverage probability analysis.



(a) Powersurface of maximum received power S , versus r_s and φ_r . (b) Powersurface of received power $S_x = g(|\phi_0^r - \phi_x|)r_x^{-\alpha_L}$, versus r_x and ϕ_x .

Fig. 3: Representative example of powersurfaces for the serving and interfering BSs corresponding to a receiver equipped with a 4-sectored antenna, $\phi_0^r = \pi/4 + \pi/2 + \pi/2$ and $S = S_{th}$.

Lemma 2. *Conditioned on the maximum received power $S = S_{th}$ from the serving BS w.r.t. a given receiving beam, the conditional Laplace transform $\mathcal{L}_I(s|S_{th}, \phi_0^r)$ of the aggregate interference power distribution is given by*

$$\mathcal{L}_I(s|S_{th}, \phi_0^r) = \exp\left(-\lambda_{bs} \int_{\Omega} \left(1 + \frac{spK g_{max} g_{3gpp}(|\phi_0^r - \phi_x|) r_x^{-\alpha_L}}{m_x}\right)^{-m_x} r_x d\Omega\right), \quad (20)$$

where $\Omega = \{(r_x, \phi_x) \in \Psi_{bs}^1 | r_x^{min} \leq r_x \leq R_L, 0 \leq \phi_x \leq 2\pi\}$ and $r_x^{min} = \min\left\{\left(\frac{g_{3gpp}(|\phi_0^r - \phi_x|)}{S_{th}}\right)^{\frac{1}{\alpha_L}}, R_L\right\}$.

Proof. Conditioned on $S = g(\varphi_r)r_s^{-\alpha_L}$, the location x_0 of the serving BS and the maxima ϕ_0^r of the receiving beam are known. The locations of $x \in \Psi_{bs}^1$, will lie outside the exclusion zone defined by all possible locations of x_0 . However, the location x_0 , given through φ_r, r_s , is a function of the maximum received power S_{th} . In Fig. 3a, a representative powersurface example of the maximum received power S from x_0 in terms of φ_r and r_s , is illustrated, by assuming a 4-sectored antenna, i.e., $\phi_{3dB} = \pi/2$. In Fig. 3b, the corresponding powersurface of the received power $S_x = g(|\phi_0^r - \phi_x|)r_x^{-\alpha_L}$ from $x \in \Psi_{bs}^1$ in terms of r_x, ϕ_x , is shown, by assuming that the third beam has been chosen as the receiving beam and therefore $\phi_0^r = \pi/4 + \pi/2 + \pi/2$. Notice that for a given value of $S = S_{th}$ in Fig. 3a, the received power from the interfering BSs should be smaller than S_{th} and the locations of $x \in \Psi_{bs}^1$ must lie outside the exclusion zone indicated by red markers. Also, notice that in Fig. 3b, S_{th} indicates the maximum received power of an

interfering BS. Considering the aforementioned, the minimum distance r_x^{min} of the interferers is given by

$$g_{3gpp}(|\phi_0^r - \phi_x|)r_x^{min-\alpha_L} < \underbrace{g(\varphi_r)r_s^{-\alpha_L}}_{S_{th}} \Leftrightarrow \frac{g_{3gpp}(|\phi_0^r - \phi_x|)}{S_{th}} < r_x^{min-\alpha_L} \Leftrightarrow r_x^{min} > \left(\frac{g_{3gpp}(|\phi_0^r - \phi_x|)}{S_{th}} \right)^{\frac{1}{\alpha_L}}, \quad (21)$$

as $\phi_x \in [0, 2\pi]$. Now, by observing from Fig. 3b that $r_x > R_L$ for some values of S , r_x^{min} is rewritten as $r_x^{min} = \min \left\{ \left(\frac{g_{3gpp}(|\phi_0^r - \phi_x|)}{S_{th}} \right)^{\frac{1}{\alpha_L}}, R_L \right\}$. Next, the Laplace transform can be obtained as shown in Appendix C. ■

The exact expression of the coverage probability for the receiver under aggregate interference can now be derived in the following Theorem.

Theorem 1. *The coverage probability of a receiver in a mmWave network inside $\mathbf{b}(\mathbf{o}, R_L)$ under the maximum power-based association policy is given by*

$$\mathcal{P}_c(\gamma) = \sum_{i=1}^{2^m} \sum_{k=0}^{m_s-1} \int_{w_{min}}^{\infty} \frac{(-s)^k}{k!} \left[\frac{\partial^k \mathcal{L}_{I_{tot}}(s|S_{th}, \phi_0^i)}{\partial s^k} \right]_s f_S(S_{th}) p_\phi dS_{th}, \quad (22)$$

where $s = \frac{m_s \gamma}{p g_{max} K S_{th}}$ and $\mathcal{L}_{I_{tot}}(s|S_{th}, \phi_0^i) = \exp(-\sigma^2 s) \mathcal{L}_I(s|S_{th}, \phi_0^i)$.

Proof. The conditional coverage probability is first given by

$$\begin{aligned} \mathcal{P}_c(\gamma) &= \mathbb{P} \left[\frac{p h_s g_{max} g(\varphi_r) l(\|x_0\|)}{I + \sigma^2} > \gamma \mid r_s, \phi_s, \phi_0^r \right] = \mathbb{P} \left[\frac{p h_s g_{max} K S_{th}}{I + \sigma^2} > \gamma \mid S_{th}, \phi_0^r \right] \\ &= \mathbb{P} \left[h_s > \frac{\gamma(I + \sigma^2)}{p g_{max} K S_{th}} \mid S_{th}, \phi_0^r \right] \stackrel{(a)}{=} \sum_{k=0}^{m_s-1} \frac{(-s)^k}{k!} \left[\frac{\partial^k \mathcal{L}_{I_{tot}}(s|S_{th}, \phi_0^r)}{\partial s^k} \right]_s \\ &\stackrel{(b)}{=} \sum_{i=1}^{2^m} \sum_{k=0}^{m_s-1} \int_{w_{min}}^{\infty} \frac{(-s)^k}{k!} \left[\frac{\partial^k \mathcal{L}_{I_{tot}}(s|S_{th}, \phi_0^i)}{\partial s^k} \right]_s f_S(S_{th}) p_\phi dS_{th}, \end{aligned} \quad (23)$$

where (a) follows from the ccdf of h_s , the definition of incomplete gamma function for integer values of m_s and by using $\mathbb{E}_{I_{tot}}[\exp(-sI_{tot})(sI_{tot})^k] = (-s)^k \frac{\partial^k \mathcal{L}_{I_{tot}}(s)}{\partial s^k}$, and (b) follows from deconditioning over the maximum power S and all possible receiving beam's maxima ϕ_0^r with the pdf $f_S(s_0)$ and the pmf p_ϕ , respectively. ■

B. Coverage Probability for minimum angular distance association scheme

In this scheme, the receiver searches and associates with the BS that has the minimum angular distance φ_c among all minimum angular distances detected from each beam's maxima. In this case, the receiver may lie anywhere in $\mathbf{b}(\mathbf{o}, R_L)$ and φ_c also denotes the serving angular distance.

Therefore, the serving distance $d_0 = \|x_0\|$ is now independent of the association policy and i.i.d. in $\mathbf{b}(\mathbf{o}, R_L)$ with pdf given by $f_{d_0}(d_0) = \frac{2d_0}{R_L^2}$, $d_0 \in [0, R_L]$. The pdf of φ_c is first derived.

Lemma 3. *For a receiver equipped with 2^m sectors, the pdf of the closest angular distance φ_c is given by*

$$f_{\varphi_c}(\varphi_c) = \lambda_{bs} 2^m R_L^2 \exp(-\lambda_{bs} 2^m \varphi_c R_L^2), \quad \varphi_c \in \left[0, \frac{\pi}{2^m}\right]. \quad (24)$$

Proof. Through manipulation of (4), let $r = R_L$, $\lambda = \lambda_{bs}$, $\phi = 2^{m+1}\varphi_c$ and $\varphi_c \in [0, \frac{\pi}{2^m}]$ so that $\phi \in [0, 2\pi]$. Then, $W(\phi, r) = \frac{\phi r^2}{2} = 2^m \varphi_c R_L^2$. Next, the proof follows the same steps as the proof for deriving (4). ■

Given φ_c and the maxima ϕ_0^r , the conditional Laplace transform of the aggregate interference power distribution can be derived.

Lemma 4. *Conditioned on φ_c w.r.t. ϕ_0^r , the conditional Laplace transform $\mathcal{L}_I(s|\varphi_c, \phi_0^r)$ of the aggregate interference power distribution is given by*

$$\mathcal{L}_I(s|\varphi_c, \phi_0^r) = \exp\left(-\lambda_{bs} \int_{\mathbf{V}} \left(1 - \left(1 + \frac{s p K g_{max} g_{3gpp}(|\phi_0^r - \phi_x|) r_x^{-\alpha_L}}{m_x}\right)^{-m_x}\right) r_x d\mathbf{V}\right), \quad (25)$$

where $\mathbf{V} = \{(r_x, \phi_x) \in \Psi_{bs}^! | 0 \leq r_x \leq R_L, \varphi_c \leq \phi_x \leq 2\pi\}$.

Proof. As the distance of x_0 is independent of the association scheme, the locations of $x \in \Psi_{bs}^!$ can be anywhere in angular distance larger than the serving angular distance φ_c , and therefore let $\mathbf{V} = \{(r_x, \phi_x) \in \Psi_{bs}^! | 0 \leq r_x \leq R_L, \varphi_c \leq \phi_x \leq 2\pi\}$. Then, the proof follows the same steps shown in Appendix C and hence it is omitted here. ■

The exact expression of the coverage probability can now be derived in the following Theorem.

Theorem 2. *The coverage probability of a receiver in a mmWave network inside $\mathbf{b}(\mathbf{o}, R_L)$ under a minimum angular distance-based association policy is given by*

$$\mathcal{P}_c(\gamma) = \sum_{i=1}^{2^m} \sum_{k=0}^{m_s-1} \int_0^{\frac{\pi}{2^m}} \int_0^{R_L} \frac{(-s)^k}{k!} \left[\frac{\partial^k \mathcal{L}_{I_{tot}}(s|\varphi_c, \phi_0^i)}{\partial s^k} \right]_s p_\phi f_{d_0}(d_0) f_{\varphi_c}(\varphi_c) dd_0 d\varphi_c, \quad (26)$$

where $s = \frac{m_s \gamma}{p g_{max} K g(\varphi_c) d_0^{-\alpha_L}}$ and $\mathcal{L}_{I_{tot}}(s|\varphi_c, \phi_0^i) = \exp(-\sigma^2 s) \mathcal{L}_I(s|\varphi_c, \phi_0^i)$.

Proof. The conditional coverage probability is first obtained similar to (22) as

$$\begin{aligned} \mathcal{P}_c(\gamma) &= \mathbb{P}\left[\frac{p h_s g_{max} g(\varphi_c) l(\|x_0\|)}{I + \sigma^2} > \gamma \mid \varphi_c, \phi_0^r, d_0\right] \\ &= \mathbb{P}\left[h_s > \frac{\gamma(I + \sigma^2)}{p g_{max} K g(\varphi_c) l(\|x_0\|)} \mid \varphi_c, \phi_0^r, d_0\right] = \sum_{k=0}^{m_s-1} \frac{(-s)^k}{k!} \left[\frac{\partial^k \mathcal{L}_{I_{tot}}(s|\varphi_c, \phi_0^r)}{\partial s^k} \right]_{s = \frac{m_s \gamma}{p g_{max} K g(\varphi_c) d_0^{-\alpha_L}}} \\ &\stackrel{(a)}{=} \sum_{i=1}^{2^m} \sum_{k=0}^{m_s-1} \int_0^{\frac{\pi}{2^m}} \int_0^{R_L} \frac{(-s)^k}{k!} \left[\frac{\partial^k \mathcal{L}_{I_{tot}}(s|\varphi_c, \phi_0^i)}{\partial s^k} \right]_s p_\phi f_{d_0}(d_0) f_{\varphi_c}(\varphi_c) dd_0 d\varphi_c, \end{aligned} \quad (27)$$

where (a) follows from deconditioning over the conditioned random variables φ_c, ϕ_0^r, d_0 of the conditional coverage probability. ■

C. Coverage Probability for minimum Euclidean distance association scheme

In this scheme, the receiver associates with the closest BS in Euclidean distance. Once the communication link has been established, all $x \in \Psi_{bs}^!$ interfere to the receiver with AoAs $\phi_x \sim U[-\pi, \pi]$. Conditioned on the serving distance $r_1 = \|x_0\|$, the conditional Laplace transform of the aggregate interference power distribution is obtained.

Lemma 5. *The Laplace transform of the aggregate interference power distribution conditioned on the serving distance r_1 is given by*

$$\mathcal{L}_I(s|r_1) = \exp\left(-\lambda_{bs} \int_{\mathbf{Q}} \left(1 - \left(1 + \frac{s p K g_{max} g_{3gpp}(\phi_x) r_x^{-\alpha_L}}{m_x}\right)^{-m_x}\right) r_x d\mathbf{Q}\right), \quad (28)$$

where $\mathbf{Q} = \{(r_x, \phi_x) \in \Psi_{bs}^! | r_1 \leq r_x \leq R_L, -\pi \leq \phi_x \leq \pi\}$.

Proof. The proof for deriving Lemma 5 follows similar steps as the one of Lemma 4. ■

The exact expression of the coverage probability for the receiver is now presented.

Theorem 3. *The coverage probability of a receiver in a mmWave network inside $\mathbf{b}(\mathbf{o}, R_L)$ under minimum Euclidean distance association policy is given by*

$$\mathcal{P}_c(\gamma) = \sum_{k=0}^{m_s-1} \int_0^{R_L} \frac{(-s)^k}{k!} \left[\frac{\partial^k \mathcal{L}_{I_{tot}}(s|r_1)}{\partial s^k} \right]_{s=\frac{m_s \gamma r_1^{\alpha_L}}{p K g_{max}^2}} f_{r_1}(r_1) dr_1, \quad (29)$$

where $\mathcal{L}_{I_{tot}}(s|r_1) = \exp(-\sigma^2 s) \mathcal{L}_I(s|r_1)$ and $f_{r_1}(r_1) = 2\pi \lambda_{bs} r_1 e^{-\lambda_{bs} \pi r_1^2}$, $r_1 \in [0, R_L]$.

Proof. The proof for deriving Theorem 3 follows similar steps as the proof in Theorem 1. ■

V. SPECIAL CASES: DOMINANT INTERFERER APPROACH

The dominant interferer approach has widely been exploited due to its usefulness when the exact analysis is too complicated or leads to unwieldy results. For instance, in [27]–[30], the authors capture the effect of the dominant interferer while approximating the residual interference with a mean value. In this section, in order to understand the focus on the effect of the different potential definitions of the dominant interferer on the performance analysis, the coverage performance is investigated under the assumption of neglecting all but a single dominant interferer for Policy 2 and 3. Accordingly, a performance comparison between the two dominant interferer approaches with the accurate performance of Policy 1, is conducted. To this end, the noise power is assumed to be negligible as compared to the aggregate interference experienced at

the receiver, i.e., interference-limited scenarios² are considered and coverage probability, i.e., $\mathcal{P}_c(\gamma) \triangleq 1 - F_{\text{SIR}}(\gamma)$, analysis is conducted in terms of the achieved SIR.

A. Coverage Probability Under Policy 2

By assuming that the receiver associates with the closest BS in angular distance, the dominant interferer is the second nearest BS in angular distance w.r.t the maxima of the receiving beam, as described in subsection III.E. Without loss of generality, the receiving beam's maxima is assumed to be along the x -axis.³ In this case, the received SIR is given by

$$\text{SIR} = \frac{g(|\varphi_1|)h_1d_1^{-\alpha_L}}{g(|\varphi_2|)h_2d_2^{-\alpha_L}}, \quad (30)$$

where $d_i \sim \frac{2d_i}{R_L^2}$, $i \in \{1, 2\}$ denotes the distance of the serving BS and the dominant interferer, respectively, $|\varphi_1|, |\varphi_2|$ denote the nearest and the second nearest absolute angular distances of the serving and interfering BS from the direction of the receiving beam's maximum directivity, and $h_1 = h_s, h_2 = h_x$, for notational convenience, respectively. Note that in order to define the interferer as "dominant", the angle $|\varphi_2|$ is restricted to $|\varphi_2| < \phi_A$, i.e., the dominant interferer is assumed to fall in the mainlobe part of the receiver's antenna pattern. Once the receiver attaches to the closest BS at $|\varphi_1|$, the angular distances $|\varphi_1|, |\varphi_2|$ are no longer independent. In this case, it is mathematically convenient to statistically characterize the SIR as $\text{SIR} = G \cdot W$, where $G = \frac{g(|\varphi_1|)}{g(|\varphi_2|)}$ and $W = \frac{h_1d_1^{-\alpha_L}}{h_2d_2^{-\alpha_L}}$. The pdf of G is first derived.

Lemma 6. *The pdf of G is given by*

$$f_G(g) = \frac{1}{\mathcal{P}_{|\varphi_1| < \phi_A, |\varphi_2| < \phi_A}} \times \int_{\frac{g_s}{g}}^{\frac{g_{max}}{g}} \frac{5 (\lambda_{bs} R_L^2 \phi_{3dB})^2 \sqrt{\log_{10}(\frac{g_{max}}{g_2}) \log_{10}(\frac{g_{max}}{g g_2})}}{24 g g_2 \ln(\frac{g_{max}}{g_2}) \ln(\frac{g_{max}}{g g_2})} \exp\left(\frac{\lambda_{bs} R_L^2 \phi_{3dB} \sqrt{10 \log_{10}(g_{max}/g_2)}}{2\sqrt{3}}\right) dg_2, \quad (31)$$

for $g \in [1, g_{max}/g_s]$ and $\mathcal{P}_{|\varphi_1| < \phi_A, |\varphi_2| < \phi_A} = 1 - e^{-\lambda_{bs} R_L^2 \phi_A} - \lambda_{bs} R_L^2 \phi_A e^{-\lambda_{bs} R_L^2 \phi_A}$.

²Please note, that since interference from other BSs is ignored, it results in stochastic dominance of the SIR as compared to the exact SIR of the respective policy, which implies that the dominant interferer approach yields a bound on the exact coverage probability of Policy 2 and Policy 3.

³As the scope of this section is merely to address the impact of the dominant interferer in the coverage performance of mmWave networks, the exhaustive scanning procedure for the association policy proposed in Section III.E is not considered here as the location of the dominant interferer is independent of the considered reference line.

Proof. See Appendix D. ■

Lemma 7. *The pdf of W is given by*

$$f_W(w) = \int_0^\infty \frac{4w_2^{-\frac{4}{\alpha_L}-1} (m_s m_x)^{-\frac{2}{\alpha_L}}}{w^{\frac{2}{\alpha_L}+1} \alpha_L^2 R_L^4} \times \frac{\left[\Gamma\left(\frac{2}{\alpha_L} + m_s\right) - \Gamma\left(\frac{2}{\alpha_L} + m_s, \frac{m_s w w_2}{R_L^{-\alpha_L}}\right) \right] \left[\Gamma\left(\frac{2}{\alpha_L} + m_x\right) - \Gamma\left(\frac{2}{\alpha_L} + m_x, \frac{m_x w_2}{R_L^{-\alpha_L}}\right) \right]}{\Gamma(m_s) \Gamma(m_x)} dw_2, \quad (32)$$

for $w \in (0, \infty)$.

Proof. The pdf of $W_i = h_i r_i^{-\alpha_L}$, $i \in \{1, 2\}$ is given by

$$f_{W_i}(w_i) = \int_{R_L^{-\alpha_L}}^\infty \frac{1}{y} f_{d_i}^{-\alpha_L}(y) f_{h_i}(w_i/y) dy = \frac{2m_u^{-\frac{2}{\alpha_L}} w_i^{-\frac{2}{\alpha_L}-1} \left[\Gamma\left(\frac{2}{\alpha_L} + m_u\right) - \Gamma\left(\frac{2}{\alpha_L} + m_u, \frac{m_u w_i}{R_L^{-\alpha_L}}\right) \right]}{\alpha_L R_L^2 \Gamma(m_u)}. \quad (33)$$

By setting $W_1 = WW_2$, the pdf of W is given by

$$f_W(w) = \int_0^\infty w_2 f_{W_1}(w w_2) f_{W_2}(w_2) dw_2. \quad (34)$$

After applying some simplifications, (32) yields. ■

Proposition 1. *The coverage probability in the presence of a dominant angular distance-based interferer under Policy 2 is given by*

$$\mathcal{P}_c(\gamma) = 1 - \int_0^\gamma \int_1^{\frac{g_{max}}{g_s}} \frac{1}{g} f_W(x/g) f_G(g) dg dx. \quad (35)$$

Proof. The pdf of the SIR results directly from expressing the SIR given as a product of two random variables

$$f_{SIR}(x) = \int_1^{\frac{g_{max}}{g_s}} \frac{1}{g} f_W(x/g) f_G(g) dg. \quad (36)$$

Then, $F_{SIR}(\gamma) = \int_0^\gamma f_{SIR}(x) dx$. ■

B. Coverage Probability Under Policy 3

In this scenario, according to Policy 3 the dominant interferer is the second closest BS in Euclidean distance to the receiver. In this case, the received SIR is given by

$$SIR = \frac{g_{max} h_1 r_1^{-\alpha_L}}{g(|\varphi_2|) h_2 r_2^{-\alpha_L}}, \quad (37)$$

where r_1, r_2 denote the distances of the serving and the dominant interfering BS from the receiver and $|\varphi_2|$ here denotes the absolute angular distance of the interfering node as seen from the receiver. For the dominant interferer scenario, the property of PPP is exploited: If

$|\varphi_2| \sim U[0, \pi]$, $|\varphi_2|$ remains uniform in the subset $[0, \phi_A]$ i.e., $|\varphi_2| \sim U[0, \phi_A]$. In this scenario, r_1, r_2 are dependent. The SIR can be written as $SIR = G \cdot W$, where $G = \frac{g_{max} h_1}{g(|\varphi_2|) h_2}$ and $W = \frac{r_1^{-\alpha_L}}{r_2^{-\alpha_L}}$.

Lemma 8. *The pdf of G is given by*

$$f_G(g) = \frac{5\sqrt{3} \left(\frac{m_s}{g_{max}}\right)^{m_s} m_x^{m_x} \phi_{3dB}}{6\sqrt{10} \ln(10) \Gamma(m_s) \Gamma(m_x) \phi_A} \int_0^\infty \int_{\frac{z}{g_{max}}}^{\frac{z}{g_s}} \frac{(gz)^{m_s-1} e^{-\frac{m_s gz}{g_{max}} - m_x x} x^{m_x-1}}{\sqrt{\log_{10}(xg_{max}/z)}} dx dz. \quad (38)$$

Proof. Following the same lines as in Appendix B, the pdf of $f_{g(|\varphi_2|)}(g_2)$ is given by

$$f_{g(|\varphi_2|)}(g_2) = \frac{5\sqrt{3} \phi_{3dB}}{6\sqrt{10} \ln(10) \phi_A g \sqrt{\log_{10}(g_{max}/g)}}, \quad g \in [g_s, g_{max}]. \quad (39)$$

Then, $f_G(g)$ can be obtained by following similar steps with the proof for Lemma 7. ■

Lemma 9. *The pdf of W is given by*

$$f_W(w) = \frac{\left(\frac{1}{w}\right)^{\frac{2+\alpha_L}{\alpha_L}} \left(\frac{3\text{erf}(\sqrt{\pi\lambda_{bs}})}{2\lambda_{bs}} - 2(1 + R_L^2 \lambda_{bs} \pi) e^{-R_L^2 \lambda_{bs} \pi} - e^{-\lambda_{bs} \pi}\right)}{\alpha_L}, \quad w \in [1, \infty), \quad (40)$$

where $\text{erf}(\cdot)$ denotes the error function [33, eq. (8.250.1)].

Proof. The joint pdf of $f_{r_1, r_2}(r_1, r_2)$ is first derived. By exploiting theory of order statistics and following similar procedure as in Appendix A, the joint pdf of $f_{r_1, r_2}(r_1, r_2)$ is given by

$$f_{r_1, r_2}(r_1, r_2) = 4(\pi \lambda_{bs})^2 r_1 r_2 e^{-\lambda_{bs} \pi r_2^2}, \quad r_1 \in [0, R_L], \quad r_2 \in [r_1, R_L]. \quad (41)$$

Then, the pdf of W is obtained by first obtaining the pdf of $v = r_1/r_2$ and then through the transformation $W = v^{-\alpha_L}$. ■

Proposition 2. *The coverage probability in the presence of a dominant interferer under Policy 3 is given by*

$$\mathcal{P}_c(\gamma) = 1 - \int_0^\gamma \int_1^\infty \frac{1}{g} f_W(x/g) f_W(g) dg dx. \quad (42)$$

Proof. The proof follows the same steps as the proof in Proposition 1. ■

VI. RESULTS AND DISCUSSION

In this section, numerical results are presented to evaluate and compare the performance achieved in a dense mmWave cellular network under different association policies. The accuracy of the analytical results is verified by comparing them with the empirical results obtained from Monte-Carlo simulations. For all numerical results, the following parameters have been used unless otherwise stated: $R_L = 75$ meters, $\alpha_L = 2$, $f_c = 26.5$ GHz as in [17]. As per the 3GPP

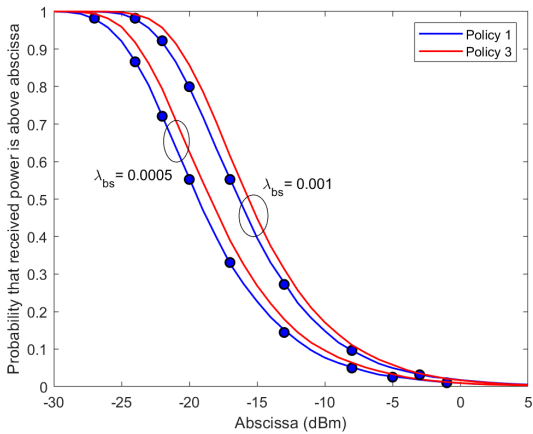


Fig. 4: Ccdf of received power under Policy 1 and Policy 3, for different values of λ_{bs} . Markers denote the analytical results.

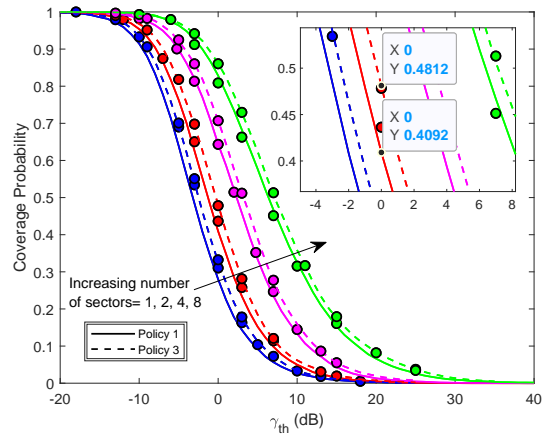


Fig. 5: Coverage probability versus γ_{th} under Policy 1 and Policy 3, for different number of sectors. Markers denote the analytical results.

specifications $p = 45$ dBm, $\sigma^2 = -74$ dBm, $\lambda_{bs} = 0.0008$ BSs/m² and $m_u = 2$. The receiver is assumed to be equipped with a directional antenna with 4 sectors, i.e., $m = 2$ and $\phi_{3dB} = \pi/2$.

Fig. 4 presents the ccdf of the maximum received power under Policy 1, defined as in (20) and evaluated through Lemma 1, for different values of λ_{bs} . To address and highlight the impact of realistic association schemes in the performance of mmWave networks, the results are compared through simulations to the received power of Policy 3, defined as $S_r = g_{max}r_1^{-\alpha_L}$, where the receiver is associated to the nearest LOS BS and no misalignment error exists. It is observed that Policy 3 overestimates the received power compared to the maximum received power achieved under Policy 1, especially for small values of the abscissa. Interestingly, notice that the misalignment error exists even in denser mmWave networks. Consequently, associating to the nearest LoS BS is not realistic, even in dense mmWave networks.

Fig. 5 compares the coverage probability versus γ_{th} under Policy 1 and Policy 3 for several numbers of beams/sectors produced by the receiver antenna. It is observed that the coverage performance of the network under Policy 3 is overestimated and the difference in coverage performance is not negligible (e.g. for $\gamma_{th} = 0$ dB, the coverage probability under Policy 3 is 0.48, while the coverage probability under Policy 1 is hardly 0.4). Note that in Policy 1, the receiver performs exhaustive scanning in each sector to select the BS that provides the maximum power. The number of beams/sectors of the receiver's antenna affects both the desired received

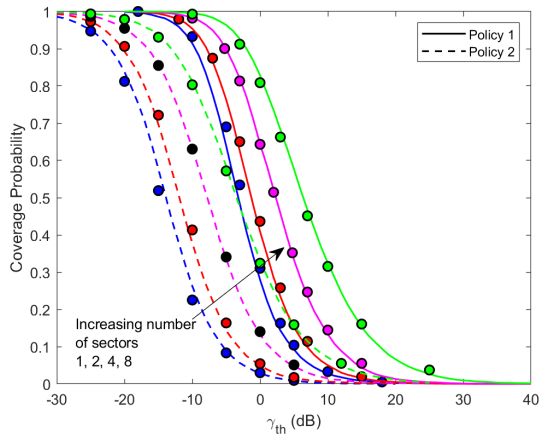


Fig. 6: Coverage probability versus γ_{th} under Policy 1 and Policy 2, for several numbers of sectors. Markers denote the analytical results.

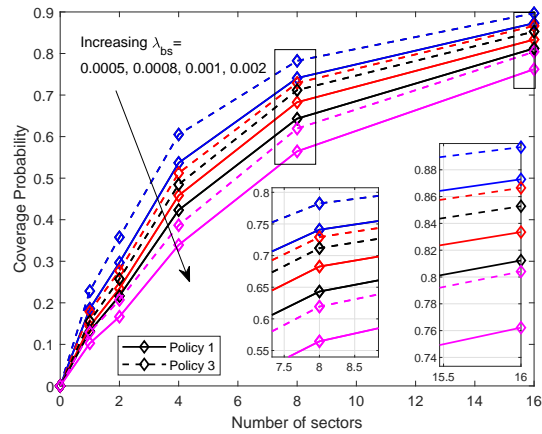


Fig. 7: Coverage probability versus number of sectors under Policy 1 and Policy 3, for different values of λ_{bs} and $\gamma_{th} = 3$ dB.

power and the interference power falling within the 3dB beamwidth of the receiver's antenna pattern, while in Policy 3 the number of sectors only determines the interference power. Indeed, by increasing the number of sectors in Policy 1, the receiver minimizes the misalignment error. At the same time, the receiver's beams become highly-directional, thus decreasing the interference power, and the coverage performance approaches the corresponding one under Policy 3.

Fig. 6 compares the coverage probability versus γ_{th} under Policy 1 and Policy 2 when the receiver's antenna is equipped with different number of sectors. In both of the association schemes, the receiver performs maximum power-based and angular distance-based exhaustive scanning, respectively to select the serving BS. It is observed that when only angular distance-based scanning is performed, the coverage performance is significantly underestimated. This result indicates that: i) Considering merely angular distance-based criteria for estimating the coverage performance is inaccurate ii) The path-loss plays a crucial role in the performance of mmWave networks.

Fig. 7 compares the coverage probability versus the number of sectors of the receiver's antenna under Policy 1 and Policy 3, derived analytically in Theorem 1 and Theorem 3, respectively, for different values of λ_{bs} and target $\gamma_{th} = 3$ dB. One can observe that the coverage performance under ideal baseline scenario overestimates the corresponding one under Policy 1, which accounts for the misalignment error, for all BSs' deployment densities. With the increase of the number of

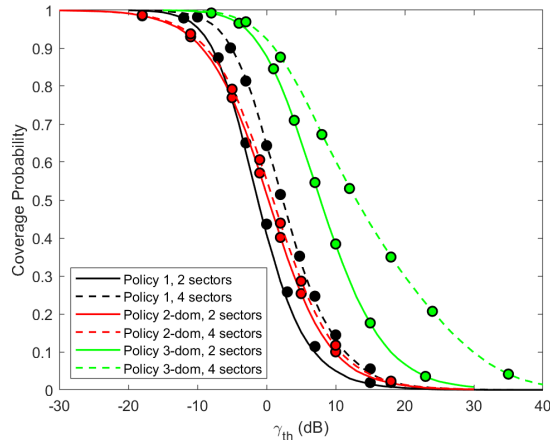


Fig. 8: Coverage probability versus γ_{th} under Policy 1 and Policy 2 and Policy 3 dominant interferer approach, for different number of sectors. Markers denote the analytical results.

sectors, the UE's beams in Policy 1 become more directional which alleviates beam misalignment effects and the coverage performance approaches the corresponding one under the ideal baseline scenario. This also highlights the need for explicitly modeling of misalignment error for realistic antenna patterns, even a small misalignment error will impact the performance and hence, the angular distances become crucial in realistic performance analysis of mmWave networks.

Fig. 8 shows the coverage probability versus γ_{th} under Policy 2 and Policy 3 for the dominant interferer. Moreover, the coverage performance under Policy 1 and aggregate interference is depicted, when the receiver's antenna is equipped with different number of sectors. Quite interestingly, it is observed that the coverage performance under Policy 2 with a single dominant interferer approximates the performance under Policy 1 with aggregate interference, especially when the number of sectors is small. In this case, the angular distance-based criterion results in realistic network performance. On the other hand, the performance under Policy 3 in the presence of a single dominant interferer clearly overestimates the corresponding one under Policy 1, which leads to the following system-level outcome: *In a LOS ball of a mmWave network under beam misalignment error at the receiver, by attaching to the closest BS in angular distance and considering the dominant interferer as the closest BS in angular distance w.r.t. the line of communication link, results in a more accurate approximation of the coverage performance compared to the policy of attaching to the closest LOS BS and considering the dominant interferer as the second nearest BS.*

VII. CONCLUSIONS

In this work, a novel stochastic geometry framework was proposed for mmWave cellular networks to address the role of the angular distances in a maximum power based association policy under a realistic beam management procedure. This necessitated the inclusion of both angular and Eudclidean distances in the analysis of cell association, which is a key novelty of this paper. Three association policies were considered for comparison: i) a realistic maximum power-based policy, ii) an angular distance-based policy, and iii) a minimum distance-based policy. Accordingly, coverage probability analysis was conducted under the three association policies and exact-form expressions were derived. Subsequently, the definition for the dominant interferer in mmWave networks is reconsidered and coverage probability analysis is performed under the dominant interferer approach for Policy 2 and Policy 3. As a key system-level insight, it was shown that considering merely Euclidean distance-based policy for determining both the serving and the dominant interfering BS, even in a LOS ball in mmWave networks, is inaccurate. Moreover, the impact of angular distances in the misalignment error was addressed. Indeed, by considering realistic antenna patterns for capturing the misalignment errors, even small error will impact the received signal power and hence angular distances play a key role in realistic performance analysis of mmWave networks.

APPENDIX A

PROOF OF (5)

Suppose that K points of Φ fall into a ball $b(o, r)$ of radius r centered at the origin o . Following the properties of a PPP, the spatial locations of the K points in $b(o, r)$ form a finite PPP and the number of points falling in $b(o, r)$ follows a Poisson distribution with mean $\lambda|b(o, r)|$. The set of the unordered absolute angular distances $\{|\phi_k|\}_{k=1:K}$ for the k th angular distance of k th point, is uniformly distributed on $[0, \pi]$, i.e., $|\phi_k| \sim U[0, \pi]$. By order statistics [40], the joint pdf of the smallest two random variables X_1, X_2 is given by

$$f_{X_1, X_2}(x, y | K) = K(K-1)[1 - F_{X_1}(y)]^{K-2} f_{X_1}(x) f_{X_1}(y). \quad (43)$$

Let $X_1 = |\varphi_1|$, $X_2 = |\varphi_2|$. Then $f_{|\varphi_1|, |\varphi_2|}(|\varphi_1|, |\varphi_2| | K)$ is given by

$$f_{|\varphi_1|, |\varphi_2|}(|\varphi_1|, |\varphi_2| | K) = \frac{K(K-1)}{\pi^2} \left(1 - \frac{|\varphi_2|}{\pi}\right)^{K-2}, \quad (44)$$

and corresponding cdf is given by

$$\begin{aligned} F_{|\varphi_1|,|\varphi_2|}(|\varphi_1^0|, |\varphi_2^0| | K) &= \int_0^{|\varphi_1^0|} \int_{|\varphi_1|}^{|\varphi_2^0|} f_{|\varphi_1|,|\varphi_2|}(|\varphi_1|, |\varphi_2| | K) d|\varphi_2| d|\varphi_1| \\ &= \frac{K}{\pi^K} \left(\frac{\pi^K - (\pi - |\varphi_1^0|)^K - K|\varphi_1^0|(\pi - |\varphi_2^0|)^{K-1}}{K} \right). \end{aligned} \quad (45)$$

Now, to obtain $F_{|\varphi_1|,|\varphi_2|}(|\varphi_1^0|, |\varphi_2^0|)$, it is required to decondition over the probability that K points fall in $b(o, r)$ and average over K , that is

$$\begin{aligned} F_{|\varphi_1|,|\varphi_2||r}(|\varphi_1^0|, |\varphi_2^0| | r) &= \sum_{k=0}^{\infty} F_{|\varphi_1|,|\varphi_2|}(|\varphi_1^0|, |\varphi_2^0| | k) \frac{(\lambda\pi r^2)^k}{k!} e^{-\lambda\pi r^2} \\ &= 1 - e^{-\lambda r^2 |\varphi_1^0|} - \lambda r^2 |\varphi_1^0| e^{-\lambda r^2 |\varphi_2^0|}. \end{aligned} \quad (46)$$

Finally, $f_{|\varphi_1|,|\varphi_2||r}(|\varphi_1|, |\varphi_2| | r)$ can be obtained after differentiating (46) w.r.t $|\varphi_1^0|, |\varphi_2^0|$ as

$$f_{|\varphi_1|,|\varphi_2||r}(|\varphi_1|, |\varphi_2| | r) = \frac{\partial^2 F_{|\varphi_1|,|\varphi_2||r}(|\varphi_1^0|, |\varphi_2^0| | r)}{\partial |\varphi_1^0| \partial |\varphi_2^0|}, \quad (47)$$

which directly results to (5).

APPENDIX B

PROOF OF LEMMA 1

The pdf of S_x is first derived. Since $\varphi_r \sim U[0, \frac{\phi_{3dB}}{2}]$, $g(\varphi_r) = 10^{\frac{G_{max}-12(\frac{\varphi_r}{\phi_{3dB}})^2}{10}}$. Then, $g(\varphi_r)$ is a function of the random variable φ_r . Building on φ_r and applying successive change of variables, the pdf $f_{g(\varphi_r)}(g)$ is given by

$$f_{g(\varphi_r)}(g) = \frac{1}{\ln(10)x} \frac{10}{12\sqrt{\frac{G_{max}-10\log(x)}{12}}}, \quad x \in [g_{3dB}, g_{max}]. \quad (48)$$

subsequently, the pdf of $r_x^{-\alpha_L}$ is expressed in terms of the corresponding cdf as

$$\begin{aligned} \mathbb{P}[r_x^{-\alpha_L} \leq x] &= \mathbb{P}\left[r_x^{\alpha_L} \geq \frac{1}{x}\right] = 1 - \mathbb{P}\left[r_x \leq \left(\frac{1}{x}\right)^{\frac{1}{\alpha_L}}\right] \\ &= 1 - F_{r_x}\left(\left(\frac{1}{x}\right)^{\frac{1}{\alpha_L}}\right), \quad F_{r_x}(r) = \frac{r^2}{R_L^2}. \end{aligned} \quad (49)$$

Now, $f_{r_x^{-\alpha_L}}(x)$ is obtained after differentiating (49) w.r.t the appropriate range of x , that is,

$$f_{r_x^{-\alpha_L}}(x) = \frac{2\left(\frac{1}{x}\right)^{\frac{\alpha_L+2}{\alpha_L}}}{\alpha_L R_L^2}, \quad x \in [R_L^{-\alpha_L}, \infty). \quad (50)$$

The pdf and the cdf of S_x can now be written as

$$f_{S_x}(w) = \int_{g_{3dB}}^{\psi(w)} \frac{1}{x} f_{g(\varphi_r)}(x) f_{r_x^{-\alpha_L}}\left(\frac{w}{x}\right) dx, \quad (51)$$

$$F_{S_x}(w_0) = \int_{g_{3dB} R_L^{-\alpha_L}}^{w_0} \int_{g_{3dB}}^{\psi(w)} \frac{1}{x} f_{g(\varphi_r)}(x) f_{r_x^{-\alpha_L}}\left(\frac{w}{x}\right) dx dw, \quad (52)$$

The pdf of $S = \max_{x \in \Psi_{bs}} \{S_x\}$ can now be obtained by exploiting theory of Order Statistics [40]. Let T_k define the event $T_k = \{k \text{ BSs exist in } \mathbf{b}(\mathbf{o}, R_L)\}$. Then, from the definition of Ψ_{bs} , $\mathbb{P}[T_k] = e^{-\lambda_{bs}\pi R_L^2} (\lambda_{bs}\pi R_L^2)^k / k!$. Given T_k and since the elements of P_{r_x} are i.i.d., the probability that $S \leq s_0$ is given by $\mathbb{P}[S \leq s_0 | T_k] = F_S(s_0 | T_k) = (F_{S_x}(w))^k$. Now, $F_S(s_0)$ can be obtained by deconditioning over T_k , that is

$$\begin{aligned} F_S(s_0) &= F_S(s_0 | T_k) \mathbb{P}[T_k] \\ &\stackrel{(a)}{=} \sum_{k=0}^{\infty} (F_{S_x}(w))^k e^{-\lambda_{bs}\pi R_L^2} \frac{(\lambda_{bs}\pi R_L^2)^k}{k!} \\ &\stackrel{(b)}{=} e^{-\lambda_{bs}\pi R_L^2} (1 - F_{S_x}(s_0)), \quad s_0 \in [w_{min}, \infty), \end{aligned} \quad (53)$$

where (a) follows after averaging over k and (b) follows from $\sum_{k=0}^{\infty} \frac{a^k b^k}{k!} \stackrel{\text{conv}}{=} e^{ab}$. Finally, the pdf $f_S(s_0)$ is obtained as $f_S(s_0) = \frac{dF_S(s_0)}{ds_0} = \lambda_{bs}\pi R_L^2 f_{P_{r_x}}(s_0) e^{\lambda_{bs}\pi R_L^2 (F_{S_x}(s_0) - 1)}$.

APPENDIX C

PROOF OF LEMMA 2

Letting $\Omega = \{(r_x, \phi_x) \in \Psi_{bs}^! | r_x^{min} \leq r_x \leq R_L, 0 \leq \phi_x \leq 2\pi\}$, the Laplace transform of I conditioned on S and ϕ_0^r is given by

$$\begin{aligned} \mathcal{L}_I(s | S_{th}, \phi_0^r) &= \mathbb{E}_{\Psi_{bs}^!} [e^{-sI}] = \mathbb{E}_{\Psi_{bs}^!} \left[e^{-s \sum_{x \in \Psi_{bs}^!} p h_x g_{max} g_{3gpp} (|\phi_0^r - \phi_x|)^l (||x||)} \middle| S_{th}, \phi_0^r \right] \\ &\stackrel{(a)}{=} \mathbb{E}_{\Psi_{bs}^!} \left[\prod_{x \in \Psi_{bs}^!} \left(1 + \frac{s p g_{max} g_{3gpp} (|\phi_0^r - \phi_x|) K r_x^{-\alpha_L}}{m_x} \right)^{-m_x} \middle| S_{th}, \phi_0^r \right] \\ &\stackrel{(b)}{=} \exp \left(\lambda_{bs} \int_{\Omega} \left(1 - \left(1 + \frac{s p g_{max} g_{3gpp} (|\phi_0^r - \phi_x|) K r_x^{-\alpha_L}}{m_x} \right)^{-m_x} \right) r_x d\Omega \right) \\ &\stackrel{(c)}{=} \exp \left(-\lambda_{bs} \int_{r_x^{min}}^{R_L} \int_0^{2\pi} \left(1 - \left(1 + \frac{s p g_{max} g_{3gpp} (|\phi_0^r - \phi_x|) K r_x^{-\alpha_L}}{m_x} \right)^{-m_x} \right) r_x d\phi_x dr_x, \right) \end{aligned} \quad (54)$$

where (a) follows from the moment generating function (MGF) of h_x , (b) follows from the probability generating functional (PGFL) of the PPP and (c) follows from integration over the set of the region Ω .

APPENDIX D
PROOF OF LEMMA 6

Since $|\varphi_1|, |\varphi_2|$ are dependent and conditioned on $|\varphi_1| < \phi_A, |\varphi_2| < \phi_A$ within $b(o, r)$, the joint pdf $f_{|\varphi_1|, |\varphi_2||R_L}(|\varphi_1|, |\varphi_2| | |\varphi_1| < \phi_A, |\varphi_2| < \phi_A | R_L)$ of $|\varphi_1|, |\varphi_2|$ is given as

$$\begin{aligned} & f_{|\varphi_1|, |\varphi_2||R_L}(|\varphi_1|, |\varphi_2| | |\varphi_1| < \phi_A, |\varphi_2| < \phi_A | R_L) \\ &= \frac{1}{P_{|\varphi_1| < \phi_A, |\varphi_2| < \phi_A}} \frac{\partial^2 F_{|\varphi_1|, |\varphi_2||R_L}(|\varphi_1^0|, |\varphi_2^0|, |\varphi_1| < \phi_A, |\varphi_2| < \phi_A | R_L)}{\partial |\varphi_1^0| \partial |\varphi_2^0|}, \end{aligned} \quad (55)$$

where $F_{|\varphi_1|, |\varphi_2||R_L}(|\varphi_1^0|, |\varphi_2^0|, |\varphi_1| < \phi_A, |\varphi_2| < \phi_A | R_L)$ is obtained through (46) for $|\varphi_1^0| < \phi_A, |\varphi_2^0| < \phi_A$ and $p_{|\varphi_1| < \phi_A, |\varphi_2| < \phi_A} = 1 - e^{-\lambda_{bs} R_L^2 \phi_A} - \lambda_{bs} R_L^2 \phi_A e^{-\lambda_{bs} R_L^2 \phi_A}$. Then, (55) is expressed through (5) as

$$\begin{aligned} f_{|\varphi_1|, |\varphi_2||R_L}(|\varphi_1|, |\varphi_2| | |\varphi_1| < \phi_A, |\varphi_2| < \phi_A | R_L) &= \frac{f_{|\varphi_1|, |\varphi_2||R_L}(|\varphi_1|, |\varphi_2|, |\varphi_1| < \phi_A, |\varphi_2| < \phi_A | R_L)}{P_{|\varphi_1| < \phi_A, |\varphi_2| < \phi_A}} \\ &= \frac{(\lambda_{bs} R_L^2)^2 e^{-\lambda_{bs} R_L^2 |\varphi_2|}}{1 - e^{-\lambda_{bs} R_L^2 \phi_A} - \lambda_{bs} R_L^2 \phi_A e^{-\lambda_{bs} R_L^2 \phi_A}}, \end{aligned} \quad (56)$$

for $|\varphi_1| \in [0, \phi_A]$ and $|\varphi_2| \in [|\varphi_1|, \phi_A]$. Now, notice that $g(|\varphi_1|), g(|\varphi_2|)$ are functions of a random variable, i.e., $g(|\varphi_i|) = g_{max} 10^{-\frac{10}{3} \left(\frac{2|\varphi_i|}{\phi_{3dB}} \right)^2}$, $i \in \{1, 2\}$. Building on $|\varphi_1|, |\varphi_2|$ and applying successive change of variables and simplifications, the joint pdf $f_{g(|\varphi_1|), g(|\varphi_2|)}(g_1, g_2)$ is given by

$$\begin{aligned} & f_{g(|\varphi_1|), g(|\varphi_2|)}(g_1, g_2) \\ &= \frac{5 (\lambda_{bs} R_L^2 \phi_{3dB})^2}{24 g_1 g_2} \frac{\sqrt{\log_{10} \left(\frac{g_{max}}{g_2} \right) \log_{10} \left(\frac{g_{max}}{g_1} \right)}}{\ln \left(\frac{g_{max}}{g_2} \right) \ln \left(\frac{g_{max}}{g_1} \right)} \frac{\exp(\lambda_{bs} R_L^2 \phi_{3dB} \sqrt{10 \log_{10} (g_{max}/g_2)} / (2\sqrt{3}))}{1 - e^{-\lambda_{bs} R_L^2 \phi_A} - \lambda_{bs} R_L^2 \phi_A e^{-\lambda_{bs} R_L^2 \phi_A}}, \end{aligned} \quad (57)$$

for $g(|\varphi_1|) \in [g_s, g_{max}]$ and $g(|\varphi_2|) \in [g_s, g(|\varphi_1|)]$. Let $g(|\varphi_1|) = g_1$ and $g(|\varphi_2|) = g_2$. Through $G = \frac{g_1}{g_2}$, it comes that $g_1 = G g_2$, where $g_s \leq g_1 \leq g_{max}$. Therefore, $g_2 \in [g_s/z, g_{max}/z]$. Then, the pdf of G can be expressed as

$$f_G(g) = \int_{\frac{g_s}{g}}^{\frac{g_{max}}{g}} g_2 f_{g(|\varphi_1|), g(|\varphi_2|)}(g g_2, g_2) dg_2, \quad g \in [1, g_{max}/g_s]. \quad (58)$$

After applying some simplifications (31) yields.

REFERENCES

- [1] F. Boccardi, R. W. Heath, A. Lozano, T. L. Marzetta, and P. Popovski, "Five disruptive technology directions for 5G," *IEEE Commun. Mag.*, vol. 52, no. 2, pp. 74–80, Feb. 2014.
- [2] *NR; User Equipment (UE) Radio Transmission and Reception; Part 1: Range 1 Standalone*, document 3GPP, TS 38.101-1, Version 15.9.0, Apr. 2020.
- [3] H. Wei, N. Deng and M. Haenggi, "Performance Analysis of Inter-Cell Interference Coordination in mm-Wave Cellular Networks," *IEEE Trans. Wireless Commun.*, vol. 21, no. 2, pp. 726-738, Feb. 2022.
- [4] V. V. Chetlur and H. S. Dhillon, "Coverage and Rate Analysis of Downlink Cellular Vehicle-to-Everything (C-V2X) Communication," *IEEE Trans. Wireless Commun.*, vol. 19, no. 3, pp. 1738-1753, Mar. 2020.
- [5] S. M. Azimi-Abarghouyi, B. Makki, M. Nasiri-Kenari and T. Svensson, "Stochastic Geometry Modeling and Analysis of Finite Millimeter Wave Wireless Networks," *IEEE Trans. on Veh. Technol.*, vol. 68, no. 2, pp. 1378-1393, Feb. 2019.
- [6] J. Fan, L. Han, X. Luo, Y. Zhang and J. Joung, "Beamwidth Design for Beam Scanning in Millimeter-Wave Cellular Networks," *IEEE Trans. Veh. Technol.*, vol. 69, no. 1, pp. 1111-1116, Jan. 2020.
- [7] Z. Gu, H. Lu, M. Zhang, H. Sun and C. W. Chen, "Association and Caching in Relay-Assisted mmWave Networks: A Stochastic Geometry Perspective," *IEEE Trans. Wireless Commun.*, vol. 20, no. 12, pp. 8316-8332, Dec. 2021.
- [8] X. Shi, N. Deng, N. Zhao and D. Niyato, "Coverage Enhancement in Millimeter-Wave Cellular Networks via Distributed IRSs," *IEEE Trans. Commun.*, doi: 10.1109/TCOMM.2022.3228298.
- [9] T. -X. Zheng et al., "Physical-Layer Security of Uplink mmWave Transmissions in Cellular V2X Networks," *IEEE Trans. Wireless Commun.*, vol. 21, no. 11, pp. 9818-9833, Nov. 2022.
- [10] M. S. Zia, D. M. Blough and M. A. Weitnauer, "Effects of SNR-Dependent Beam Alignment Errors on Millimeter-Wave Cellular Networks," *IEEE Trans. on Veh. Technol.*, vol. 71, no. 5, pp. 5216-5230, May 2022.
- [11] S. Fang, G. Chen, X. Xu, S. Han and J. Tang, "Millimeter-Wave Coordinated Beamforming Enabled Cooperative Network: A Stochastic Geometry Approach," *IEEE Trans. Wireless Commun.*, vol. 69, no. 2, pp. 1068-1079, Feb. 2021.
- [12] C. Zhang, W. Yi, Y. Liu, K. Yang and Z. Ding, "Reconfigurable Intelligent Surfaces Aided Multi-Cell NOMA Networks: A Stochastic Geometry Model," *IEEE Trans. Commun.*, vol. 70, no. 2, pp. 951-966, Feb. 2022.
- [13] M. Haenggi, J. G. Andrews, F. Baccelli, O. Dousse, and M. Franceschetti, "Stochastic geometry and random graphs for the analysis and design of wireless networks", *IEEE J. Sel. Areas Commun.*, vol. 27, no. 7, pp. 1029–1046, Sep. 2009.
- [14] J. G. Andrews, F. Baccelli, and R. K. Ganti, "A tractable approach to coverage and rate in cellular networks", *IEEE Trans. Commun.*, vol. 59, no. 11, pp. 3122–3134, Nov. 2011.
- [15] H. ElSawy, E. Hossain, and M. Haenggi, "Stochastic geometry for modeling, analysis, and design of multi-tier and cognitive cellular wireless networks: A survey", *IEEE Commun. Surveys Tuts.*, vol. 15, no. 3, pp. 996–1019, 3rd Quart., 2013.
- [16] Z. Li and W. Wang, "Handover performance in dense mmWave cellular networks," in *Proc. 10th Int. Conf. Wireless Commun. Signal Process. (WCSP)*, Oct. 2018, pp. 1–7.
- [17] S. S. Kalamkar, F. Baccelli, F. M. Abinader, A. S. Marcano Fani and L. G. Uzeda Garcia, "Beam Management in 5G: A Stochastic Geometry Analysis," *IEEE Trans. Wireless Commun.*, doi: 10.1109/TWC.2021.3110785.
- [18] S. Aghashahi, S. Aghashahi, Z. Zeinalpour-Yazdi, A. Tadaion and A. Asadi, "Stochastic Modeling of Beam Management in mmWave Vehicular Networks," *IEEE Trans. Mob. Comput.*, doi: 10.1109/TMC.2021.3138449.
- [19] W. Chen, L. Li, Z. Chen, H. H. Yang and T. Q. S. Quek, "Mobility and Blockage-induced Beam Misalignment and Throughput Analysis for THz Networks," *IEEE Global Commun. Conf. (GLOBECOM)*, pp. 1-6, Dec. 2021.
- [20] M. Giordani et al., "A tutorial on beam management for 3GPP NR at mmWave frequencies," *IEEE Commun. Surveys Tuts.*, vol. 21, no. 1, pp. 173–196, 1st Quart., 2018.

- [21] N. R. Olson, J. G. Andrews and R. W. Heath, "Coverage and Capacity of Terahertz Cellular Networks With Joint Transmission," *IEEE Trans. Wireless Commun.*, vol. 21, no. 11, pp. 9865-9878, Nov. 2022.
- [22] M. Rebato, J. Park, P. Popovski, E. De Carvalho and M. Zorzi, "Stochastic Geometric Coverage Analysis in mmWave Cellular Networks With Realistic Channel and Antenna Radiation Models," *IEEE Trans. Commun.*, vol. 67, no. 5, pp. 3736-3752, May 2019.
- [23] M. Banagar and H. S. Dhillon, "3D Two-Hop Cellular Networks With Wireless Backhauled UAVs: Modeling and Fundamentals," *IEEE Trans. Wireless Commun.*, vol. 21, no. 8, pp. 6417-6433, Aug. 2022.
- [24] X. Yu, J. Zhang, M. Haenggi, and K. B. Letaief, "Coverage analysis for millimeter wave networks: The impact of directional antenna arrays," *IEEE J. Sel. Areas Commun.*, vol. 35, no. 7, pp. 1498–1512, Jul. 2017.
- [25] N. Deng and M. Haenggi, "A Novel Approximate Antenna Pattern for Directional Antenna Arrays," *IEEE Wireless Commun. Lett.*, vol. 7, no. 5, pp. 832-835, Oct. 2018.
- [26] W. Yi, Y. Liu, Y. Deng and A. Nallanathan, "Clustered UAV Networks With Millimeter Wave Communications: A Stochastic Geometry View," *IEEE Trans. Wireless Commun.*, vol. 68, no. 7, pp. 4342-4357, Jul. 2020
- [27] J. Schloemann, H. S. Dhillon, and R. M. Buehrer, "Toward a tractable analysis of localization fundamentals in cellular networks," *IEEE Trans. Wireless Commun.*, vol. 15, no. 3, pp. 1768–1782, Mar. 2016.
- [28] V. V. Chetlur and H. S. Dhillon, "Downlink Coverage Analysis for a Finite 3-D Wireless Network of Unmanned Aerial Vehicles," *IEEE Trans. Commun.*, vol. 65, no. 10, pp. 4543-4558, Oct. 2017.
- [29] T. Bhandari, H. S. Dhillon, and R. M. Buehrer, "The impact of proximate base station measurements on localizability in cellular systems," in *Proc. IEEE SPAWC*, Edinburgh, U.K., Jul. 2016.
- [30] M. A. Kishk and H. S. Dhillon, "Joint Uplink and Downlink Coverage Analysis of Cellular-based RF-powered IoT Network", *IEEE Trans. Green Commun. Netw.*, vol. 2, no. 2, pp. 446-459, Jun. 2018.
- [31] A. G. Kanatas, "Coordinates Distributions in Finite Uniformly Random Networks," *IEEE Access*, vol. 10, pp. 49005-49014, 2022.
- [32] C. K. Armeniakos and A. G. Kanatas, "Angular Distance-Based Performance Analysis of mmWave Cellular Networks," *IEEE Global Commun. Conf. (GLOBECOM)*, pp. 5432-5437, Dec. 2022.
- [33] I. Gradshteyn and I. M. Ryzhik, "*Tables of Integrals, Series, and Products*," 7th ed. New York, NY, USA: Academic, 2007.
- [34] M. Rebato, L. Resteghini, C. Mazzucco and M. Zorzi, "Study of Realistic Antenna Patterns in 5G mmWave Cellular Scenarios," in *IEEE Int. Conf. Commun.*, 2018, pp. 1-6
- [35] J. Wildman, P. H. J. Nardelli, M. Latva-aho and S. Weber, "On the Joint Impact of Beamwidth and Orientation Error on Throughput in Directional Wireless Poisson Networks," *IEEE Trans. Wireless Commun.*, vol. 13, no. 12, pp. 7072-7085, Dec. 2014.
- [36] A. Thornburg, T. Bai and R. W. Heath, "Performance Analysis of Outdoor mmWave Ad Hoc Networks," *IEEE Trans. Signal Process.*, vol. 64, no. 15, pp. 4065-4079, Aug. 2016
- [37] J. G. Andrews, T. Bai, M. N. Kulkarni, A. Alkhateeb, A. K. Gupta, and R. W. Heath, "Modeling and analyzing millimeter wave cellular systems," *IEEE Trans. Commun.*, vol. 65, no. 1, pp. 403–430, Jan. 2017
- [38] K. Humadi, I. Trigui, W. -P. Zhu and W. Ajib, "User-Centric Cluster Design and Analysis for Hybrid Sub-6GHz-mmWave-THz Dense Networks," *IEEE Trans. Veh. Technol.*, vol. 71, no. 7, pp. 7585-7598, Jul. 2022.
- [39] T. Bai and R. W. Heath, "Coverage and rate analysis for millimeterwave cellular networks," *IEEE Trans. Wireless Commun.*, vol. 14, no. 2, pp. 1100–1114, Feb. 2015.
- [40] M. Ahsanullah, V. Nevzorov and M. Shakil, *An Introduction to Order Statistics*. Atlantis Press, 2013.